

High-performance CO₂-philic graphene oxide membranes in the wet-conditions

Hyo Won Kim,^a Hee Wook Yoon,^a Byung Min Yoo,^a Jae Sung Park,^b Kristofer L. Gleason,^b
Benny D. Freeman,^b and Ho Bum Park^{a,*}

^aDepartment of Energy Engineering, Hanyang University, Seoul, 133-791, Republic of Korea

^bDepartment of Chemical Engineering, Center for Energy and Environmental Resources,
University of Texas at Austin, 10100 Burnet Road, Building 133 Austin, Texas 78758,
United States

*Corresponding author (badtzhb@hanyang.ac.kr)

Experimental Section

Materials Fine grade synthetic graphite powder (SP-1) was supplied by Bay Carbon Inc. (Bay City, MI, USA) and used as received. Sulphuric acid (H_2SO_4 , 97%), hydrochloric acid (HCl , 35% in water), acetone (CH_3COCH_3 , 99.5%) from Daejung Chemicals & Metals Co. (Siheung, Korea), hydrogen peroxide (H_2O_2 , 50% in water), phosphorous pentoxide (P_2O_5 , 98%), and potassium permanganate (KMnO_4) from Junsei Chemical Co. (Tokyo, Japan) were also used as received. Porous poly(ether sulfones) (PES, Sepro Membranes Inc., Oceanside, CA, USA) were used as a substrate to prepare the GO membranes.

GO synthesis GO was synthesized using the modified Hummers method.^{7, 10} Sulphuric acid (450 ml) was added to graphite powder (10 g). The temperature of the solution was maintained below 10°C and stirred for 90 min. A small amount (1.5 g) of potassium permanganate was added to the mixture and stirred for 90 min. Then, a large amount of potassium permanganate (30 g) was added to the mixture and stirred for 1 h. The solution changed in colour from black to dark green. In this step, the reaction temperature was kept below 10°C. The solution was heated to 40°C and stirred for 1 h. Deionized water (450 ml) was poured into the solution in a drop-wise fashion. The temperature was maintained below 50°C to prevent a rapid increase in temperature that could result in a thermal explosion. The solution turned brown. The solution was then heated to 95°C for 30 min, and a hydrogen peroxide solution (10 wt%, 300 ml) was poured into the solution and stirred for 30 min. The solution changed to light yellow. Synthesized graphene oxide was purified with hydrochloric acid and acetone. The GO solution was filtered and washed with hydrochloric acid (10 wt%, 5000 ml) five times. Filtered GO cakes were dried over phosphorous pentoxide at 40°C for 24 h under vacuum. The GO powders were redispersed in acetone (5000 ml) and filtered and

washed three times. The cake layer was dried at 40°C for 24 h under vacuum.

Preparation of atomic thick GO membranes The dispersed GO in water at the concentration of 1.0 mg/mL (adjusted to pH 10.0 with 1 M NaOH) was prepared and heavily sonicated with a tip sonicator (Sonics & Materials Inc., VC505, 500 W, 20kHz) for 6 h to reduce the flake size of the GO sheets for shortening the GO membrane tortuosity¹⁶. To investigate gas transport behaviour, several-layered GO membranes were prepared by spin-coating on a porous PES membrane¹¹. The microporous PES membranes were cut into 10 X 10 cm coupons and carefully attached on a flat acryl plate using Scotch Tape. The prepared PES-attached acryl plate was placed on a spin coater and spun at 3,000 rpm. One ml of GO solution was dropped at the same dropping velocity on the centre of the spinning substrate. These steps were then repeated five times.

Material Characterizations

Structure and film images Effective thickness and layering structure of the GO membranes were determined using transmittance electron microscopy (TEM) (FEI, Hillsboro, OR, USA).

Gas and water vapour adsorption/desorption isotherms of GO

Gas adsorption and desorption experiments were performed using the Brunauer-Emmett-Teller (BET) method to investigate the adsorption/desorption mechanism and properties of the GO using a surface area and porosimetry analyser (ASAP 2020, Micromeritics Instrument Corp., Norcross, GA, USA). CO₂ adsorption was measured at 273 K and 1 bar using ASAP 2020. Samples were degassed under high dynamic vacuum for 16 hours prior to measurement. Water vapour sorption experiments were performed by a dynamic vapour sorption (DVS)

apparatus (DVS-1000, Surface Measurement System Ltd., London, UK) at a varying relative humidity (RH) from 0 to 95% at 25°C.

Gas and water vapour permeation measurements

Gas separation under the dried feed state The gas transport performance of ultrathin GO membranes was determined using a constant-pressure variable volume method at an upstream pressure of 225.0 cmHg, a downstream pressure of 76.0 cmHg (i.e., atmosphere conditions) and a temperature of 25°C using a water bath for gas molecules with different kinetic diameters (e.g., H₂ (0.289 nm), O₂ (0.346 nm), N₂ (0.364 nm), CH₄ (0.384 nm), and CO₂ (0.330 nm). Gas flow rates were detected with a bubble flow-meter at a volume of 0.1 ml accepted for CO₂ (1.0 ml). The effective membrane surface area was 13.8 cm². After the system reached steady-state, all gas permeation measurements were performed more than five times and standard deviations from mean values of each permeance were within ± 2%. Gas permeance (Q) was determined using the following equation:

$$Q_A = \frac{1}{p_2 - p_1} \cdot \frac{273.15}{(273.15 + T)} \cdot \frac{p_{atm}}{76} \cdot \frac{1}{A} \cdot \left(\frac{dV}{dt}\right)$$

where p_2 is the upstream pressure, p_1 is the downstream pressure (atmosphere in this case), p_{atm} is the atmospheric pressure (atm), A is the membrane effective area, T is the temperature (Celsius), and dV/dt is the volumetric displacement rate in the bubble flow meter. The ideal separation factor (permselectivity) of two components is defined as the ratio of the measured gas permeance value:

$$\alpha = \frac{Q_1}{Q_2}$$

where Q_1 and Q_2 refer to the permeance of each species, respectively.

Water vapour transmission through GO membranes Water vapour permeance was measured in accordance with ASTM E96/E96M-10 (Standard Test Methods for Water Vapour Transmission of Materials), sections 11, 12 (the water method), and 13.4.2 (corrections for resistance due to still air). To perform a measurement, samples were masked with aluminium tape and installed in 10 cm² Payne permeability cups (Model: 1003, Sheen Instruments, UK), which were partially filled with deionized water. Composite membrane samples were installed with the GO layer facing the inside of the cup. An air space of 0.245 cm between the surface of the deionized water and the bottom side of each sample was maintained in order to prevent water from contacting the samples when cups were handled. The cups were placed into an environmental chamber (Model BTL-433, Espec North America, INC, USA) which controls the relative humidity (RH) and temperature. Since the membrane transmits water vapour while the sample is ramping from ambient humidity to the test humidity and back again, two cycles were run for each desired humidity set point to obtain the steady-state rate of mass loss. For the first cycle, the temperature was ramped from 50% RH to the set point at 1%/min, held at the set point for 30 min, ramped back down to 50% RH, and then weighed. The second cycle was identical to the first, except that the chamber was held at the set point for 24 h. All measurements were made at 25 °C. From the results of these two cycles, the steady-state rate of mass loss is:

$$\frac{d_m}{d_t} = \frac{\Delta m_2 - \Delta m_1}{\Delta t_2 - \Delta t_1}$$

where Δm_1 and Δm_2 are the changes in mass for the first and second measurements, Δt_1 and Δt_2 are the durations of the first and second measurements, respectively. It is assumed that permeation reaches steady-state within 30 mins of reaching the final set point. By subtracting these two cycles, mass loss occurring during the humidity ramps and the non-steady-state mass loss at the beginning of the hold period was excluded.

Total permeance, Q_{total} , is determined from the rate of mass change, saturation vapour pressure, and relative humidity:

$$Q_{total} = \frac{d_m}{d_t} \times [A_{film} \cdot P_{sat} \cdot (1 - RH)]^{-1}$$

where A_{film} is the area of the film samples, P_{sat} is the saturation pressure of water vapour, and RH is the relative humidity. Owing to the high water vapour flux observed for GO composite membranes, it was necessary to correct for the mass-transfer resistance of the air gap between the surface of the water and the bottom of the membrane. Permeability, P_a ($kg \cdot m^{-1} \cdot s^{-1} \cdot Pa^{-1}$) of the still air layer in the cup is given by following equation:

$$P_a = \frac{2.306 \times 10^{-5} \cdot P_0}{R_v \cdot T \cdot P} \cdot \left(\frac{T}{273.15} \right)^{1.81}$$

where T is the temperature (K), P is the ambient pressure (Pa), P_0 is standard atmospheric pressure (i.e. $1.01325 \times 10^6 \cdot Pa$), and R_v is the ideal gas constant for water (i.e., $4.615 \times 10^2 \cdot J \cdot K^{-1} \cdot kg^{-1}$). The corrected permeance, $Q_{corrected}$, is obtained assuming a series resistance model:

$$Q_{corrected}^{-1} = Q_{total}^{-1} - \frac{l}{P_a}$$

where l is the thickness of the air layer (m).

Table S1. CO₂ uptakes of various porous materials. The high CO₂ sorption nature of GO is caused by polar functional groups, such as –OH, C-O-C and –COOH. According to recent studies on intermolecular interactions between the CO₂ molecule and aromatic molecules with polar functional groups,^{S1, S2} the strongest types of intermolecular interactions were found to be: (1) hydrogen bond interactions between acidic protons of COOH and CO₂ oxygen, or (2) between lone pair donating atoms (N, O) of the side groups and the C of CO₂. Also, the CO₂ uptake properties for a series of conjugated microporous polymer (CMP) networks are strongly dependence on incorporated functional groups such as –COOH, –NH₂, –OH, and –CH₃. Interestingly, carboxylic acid modified CMP shows the highest amount of CO₂ adsorption capacity, although such CMP has the lowest surface area among samples.^{S3} GO consists of a number of –OH and C-O-C groups on the basal plane and –COOH groups at the edges; that is, such polar groups contribute to high CO₂ affinity with GO sheets. In general, the gas permeability of membrane is a product of gas diffusivity and gas solubility; therefore, the enhanced CO₂ sorption capability in GO membranes leads to higher CO₂ permeability even more than in smaller molecules (e.g., H₂) with higher diffusivity.

Category	Materials	BET surface (m ² /g)	CO ₂ uptake at 1 bar (mg/g : mmol/g)	CO ₂ uptake at high pressure (mg/g : mmol/g)	References
	GO	6.0	66.9 / 1.52	72.6 / 1.65 at 27 bar	In this study
Activated carbon	BPL carbon	1250	83.6 / 1.9	370 / 8.41 at 40 bar	[24]
	Norit RB2	1180	112 / 2.5	420 / 9.55 at 40 bar	[25]
MOF	MOF-5	3800	47 / 1.1	970 / 22.0 at 40 bar	[25]
	MOF-177	4750	22 / 0.5	1490 / 33.9 at 40 bar	[25]
	IRMOF-6	2800	22 / 0.5	870 / 19.8 at 40 bar	[25]
	MIL-101(Cr)	4230	84 / 1.9	1760 / 40 at 50 bar	[25]
	MOF-2	345	25 / 0.59	143 / 3.2 at 40 bar	[25]
	IRMOF-11	2096	79 / 1.8	649 / 14.8 at 40 bar	[25]
	IRMOF-3	2160	54 / 1.2	830 / 18.9 at 40 bar	[25]
	IRMOF-6	2516	48 / 1.1	866 / 19.7 at 40 bar	[25]
	IRMOF-1	2833	47 / 1.1	968 / 22.0 at 40 bar	[25]
	MOF-177	4508	35 / 0.8	1493 / 33.9 at 40 bar	[25]
Zeolite	Zeolite 13X	615.5	176 / 4.0	324 / 7.37 at 40 bar	[S4]
	Zeolite 5A	n.a.	137 / 3.1	154 / 3.5 at 10 bar	[S4]
	MCM-41	n.a.	14.3 / 0.33	n.a.	[S4]

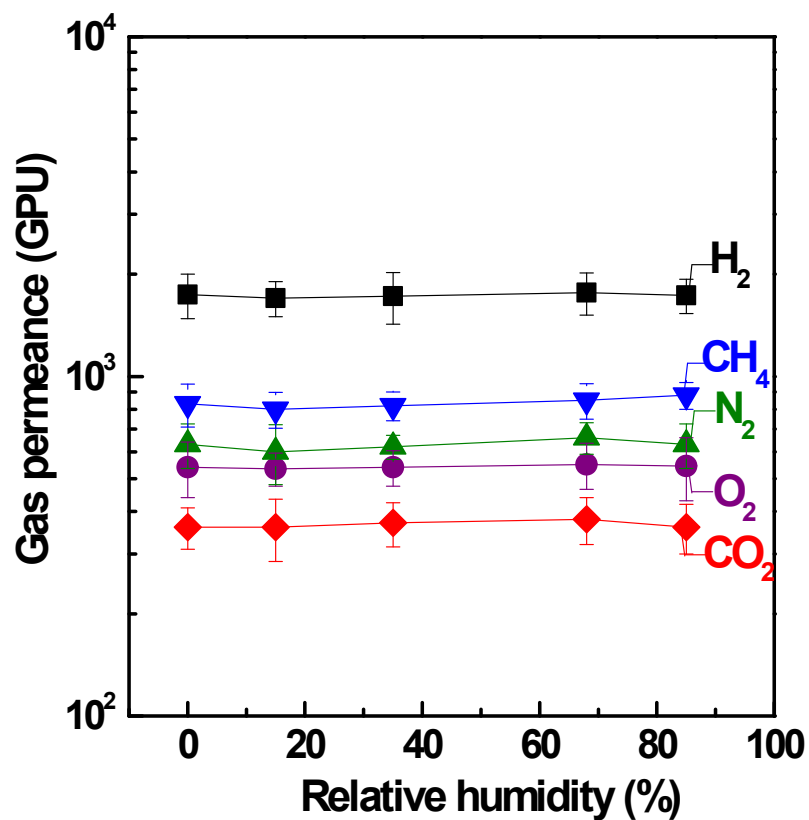


Figure S1. Gas permeances of pristine PES membranes as a function of relative humidity at 25 °C. Such pristine PES membranes exhibit independent gas permeation properties as a function of relative humidity in feed streams, owing to the relative large pore size of the PES membranes. Namely, dried and hydrated gases can freely diffuse through the porous PES membranes without any interaction between pore wall and the gas molecules under dried and humidified feed conditions.

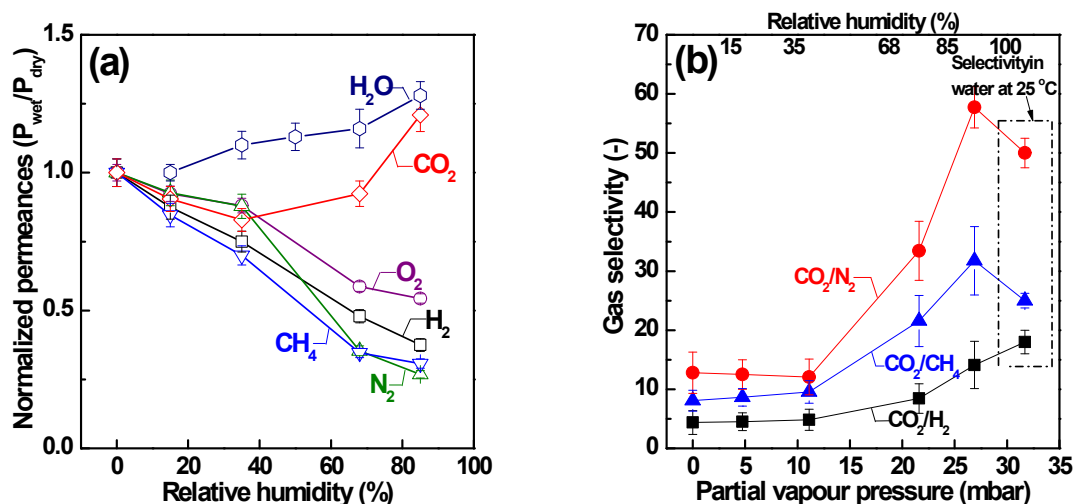


Figure S2. Gas permeances (a) and gas selectivity (b) in few-layered GO membranes depending on RH at 25°C (operating temperature) and 1 bar (applied feed pressure). RH was controlled by saturated salt solutions that are lithium chloride (12%), magnesium chloride (33%), and sodium chloride (75%). In general, all gas permeances were reduced with an increase of RH, except for CO_2 , which leads to the improvement of CO_2 /gases selectivity with increasing RH. For example, the CO_2/CH_4 selectivity of dry GO membrane increased from 8.8 to 32 in the presence of water vapour. This gas transport behavior is closely related to the presence of water molecules sorbed in interlayer spacings of multi-stacked GO sheets and the amount of intercalated water molecules. A slight decrease of CO_2 permeance at a low RH may have been due to the discontinuity of water clusters intercalated between GO sheets. Although CO_2 is highly soluble in water compared to other gas molecules, which results in enhanced CO_2 solubility, isolated water molecules also delay CO_2 diffusivity and attenuate the contribution of enhanced CO_2 solubility to gas permeability. However, at high RH, the continuum of water molecules will further increase the contribution of enhanced CO_2 solubility, which again leads to an increase of gas permeability.

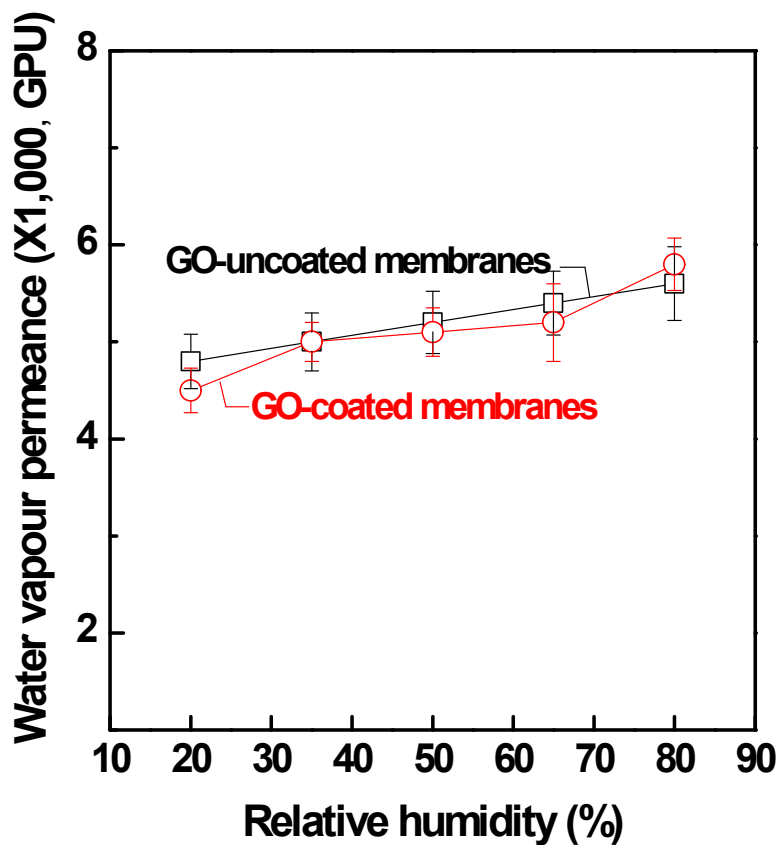


Figure S3. Water vapour permeances through few-layered GO membranes as a function of relative humidity at 25 °C. Overall, such GO membranes exhibit extremely fast water vapour permeances, and water vapour permeances of the GO membranes gradually increase with increasing relative humidity. At low relative humidity, the GO membranes show lower water permeances than pristine substrates. At high relative humidity, water vapour permeances of the GO membranes exceed that of pristine substrates owing to improved hydrophilicity, leading to enhanced solubility.

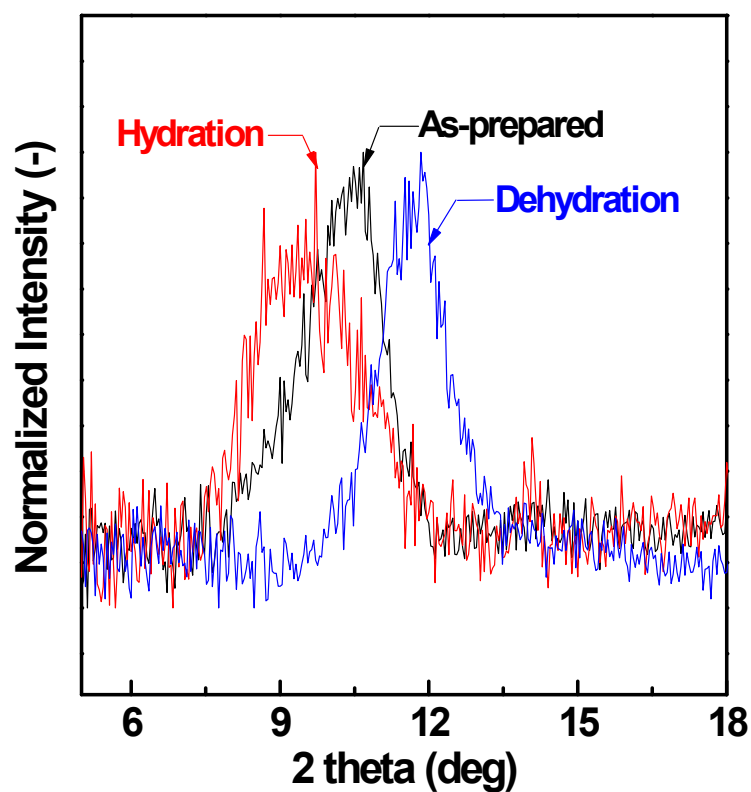


Figure S4. XRD patterns of prepared, hydrated, and dehydrated GO membranes. The intercalated water molecules can change the interlayer distances (i.e., d -spacing) in GO lamellae. The interlayer spacing of the GO membranes is increased when the GO membranes are exposed to water vapour. That is, the d -spacing of prepared, hydrated, and dehydrated GO membranes is 8.6, 10.5, and 7.8 Å, respectively, indicating that water vapour can freely diffuse in or out the interlayered spacing of GO membranes.

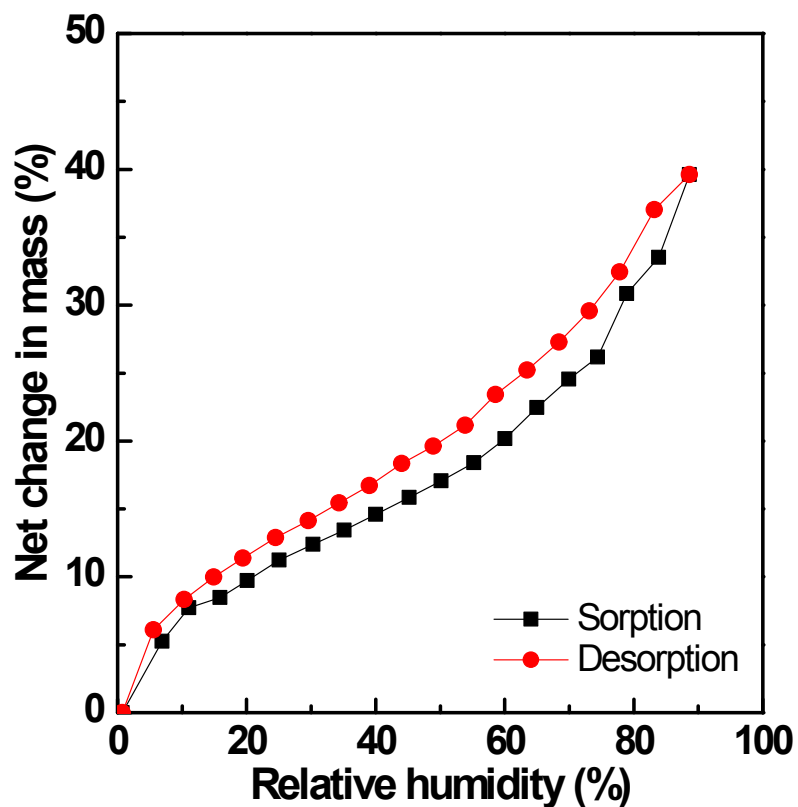


Figure S5. Water vapour adsorption/desorption isotherms for GO sheets as a function of relative humidity (RH) at 25°C by a dynamic vapour sorption (DVS) apparatus. The weight of the GO sheet strongly depends on the RH; i.e., the GO sheets show a significantly high water vapour sorption nature. Additionally, the isotherm exhibits some hysteresis, which implies that once water molecules are adsorbed on GO sheets, the trapped water in GO layers is difficult to separate from GO flakes owing to the high interaction between GO sheets and water vapour.

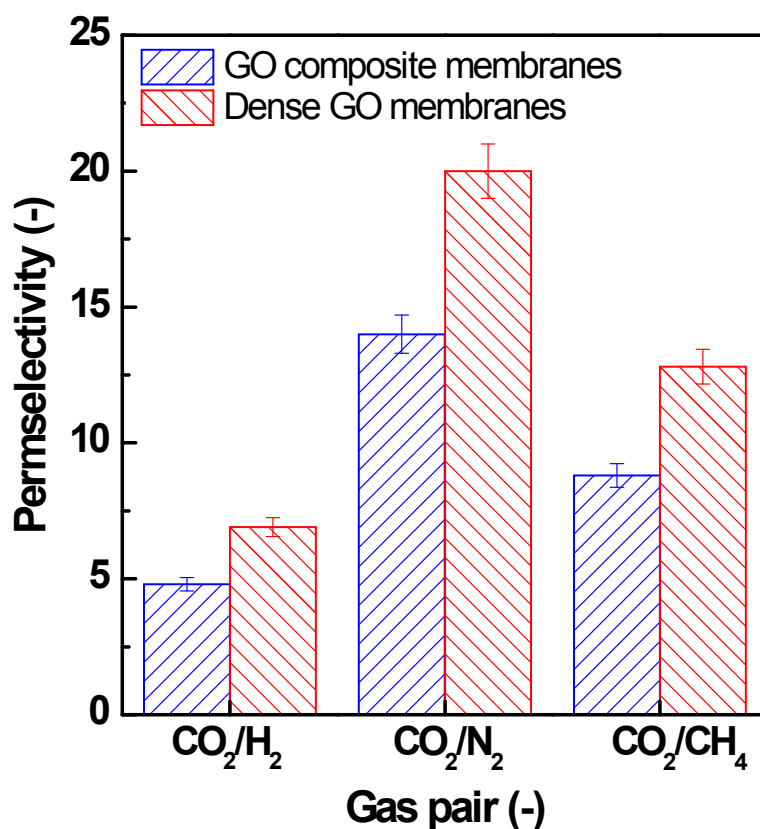


Figure S6. Permeability difference between GO composite and dense GO (calculated from resistance model) membranes due to porosity in the microporous support layers. Because asymmetric membrane structures consisting of the effective skin layer and porous substrates provide highly permeable properties, asymmetric structures with ultrathin and defect-free skin layers have been considered as the most suitable configuration in practical membrane applications. Therefore, many studies have been devoted to the development of ultrathin and defect-free skin layers. However, simulation and experimental results demonstrated that the gas separation properties of asymmetric membranes strongly depend on the permeation resistance of the substrate. A decrease in gas permeation of support layer typically leads to a dramatic decrease in the gas permeation as well as gas selectivity of asymmetric structure membranes. In particular, gas selectivity of composite membranes is gradually decreased as gas permeation of substrates is decreased because gas transport through microporous substrates is followed by Knudsen diffusion, which has a relatively poor separation ability. Therefore, gas selectivity of asymmetric membranes is substantially lower than that of the effective skin layer due to the substantial resistance of the support layer.

References

- S.1. A. Torrisi, R. G. Bell and C. Mellot-Draznieks, *Cryst. Growth Des.*, 2010, **10**, 2839-2841.
- S.2. A. Torrisi, C. Mellot-Draznieks and R. G. Bell, *J. Chem. Phys.*, 2009, **130(19)**, 194703.
- S.3. R. Dawson, D. J. Adams, A. I. Cooper, *Chem. Sci.*, 2011, **2**, 1173-1177.
- S.4. D. Bonenfant, M. Kharoune, P. Niquette, M. Mimeault, R. Hausler, *Adv. Mater.*, 2008, **9**, 013007.